Correlation slopes of GEM/CO, GEM/CO_2, and GEM/CH_4 and estimated mercury emissions in China, South Asia, Indochinese Peninsula, and Central Asia derived from observations in northwest and southwest China

X. W. Fu[1], H. Zhang[1, 2], C.-J. Lin[1,3,4], X. Feng[1,*], L. X. Zhou[5,*], S. X. Fang[5]

[1]State Key Laboratory of Environmental Geochemistry, Institute of Geochemistry, Chinese Academy of Sciences, Guiyang 550002, PR China;

[2]Graduate University of the Chinese Academy of Sciences, Beijing 100049, PR China

[3]Department of Civil Engineering, Lamar University, Beaumont, Texas 77710, United States

[4]College of Energy and Environment, South China University of Technology, Guangzhou 510006, China

[5]Chinese Academy of Meteorological Sciences (CAMS), CMA, Beijing 100081, China

* Corresponding authors, 1. X. B. Feng, e-mail address: fengxinbin@vip.skleg.cn; phone: +86 851 5895823

2. L. X. Zhou, e-mail address: zhoulx@cams.cma.gov.cn

Abstract. Correlation analysis between atmospheric mercury (Hg) and other trace gases are useful for identification of sources and constraining regional Hg emissions. Emissions of Hg in Asia contribute significantly to the global budget of atmospheric Hg. However, due to the lack of reliable data on the source strength, large uncertainties remain in the emission inventories of Hg in Asia. In the present study, we calculated the correlation slopes of GEM/CO, GEM/CO_2, and GEM/CH_4 for mainland China, South Asia, Indochinese Peninsula, and Central Asia using the ground-based observations at three remote sites in northwest and southwest China, and applied the values to estimate GEM emissions in the four source regions. The geometric mean GEM/CO correlation slopes for mainland China, South Asia, Indochinese Peninsula, and Central Asia were 7.3±4.3, 7.8±6.4, 7.8±5.0, and 13.4±9.5 pg m^{-3}/ppb, respectively, and values in the same source regions were 33.3±30.4, 27.4±31.0, 23.5±15.3, and 20.5±10.0 pg m^{-3}/ppb for the GEM/CH_4 correlation slopes, respectively. The geometric means of GEM/CO_2 correlation slopes for mainland China, South Asia and Central Asia were 240±119, 278±164, 315±289 pg m^{-3}/ppm, respectively. These values were the first reported correlation slopes of GEM/CO, GEM/CO_2, and GEM/CH_4 in four important source regions of Asia except the GEM/CO ratios in mainland China. The correlation slopes of GEM/CO, GEM/CO_2 and GEM/CH_4 in Asia were relatively higher than those observed in Europe, North America and South Africa, which may highlight GEM emissions from non-ferrous smelting, large-scale and artisanal mercury and gold productions, natural sources and historical deposited mercury (re-emission) in Asia. Using the observed GEM/CO and GEM/CO_2 slopes, and the recently reported emission inventories of CO and CO_2, the annual GEM emissions in mainland China, South Asia, Indochinese Peninsula, and Central Asia were estimated to be in the ranges of 1071-1187 tons, 340-470 tons, 125 tons, and 54-90 tons, respectively. The estimate quantity of GEM emissions from the GEM/CH_4 correlation slopes is significantly larger, which may be due to the larger uncertainties of CH_4 emissions in Asia as well as insufficient observations of GEM/CH_4 correlation slopes and therefore lead to an overestimate of GEM emissions. Our estimates of GEM emissions in the four Asian regions were significantly higher (3-4 times) than the anthropogenic GEM emissions reported by recent studies. This discrepancy could come from a combination of reasons including underestimates of anthropogenic and natural GEM emissions, large uncertainties related to CO, CO_2, and CH_4 emission inventories, and inherent limitations of the correlation slopes method.

1 Introduction

Mercury (Hg) is a persistent pollutant in the environment and poses health risks for human health mainly by consuming fish. Due to primary- and re-emissions of Hg from anthropogenic sources, global atmospheric Hg budget has increased significantly since the industrial revolution (Mason et al., 1994). There are three major operationally defined Hg forms in the atmosphere, namely elemental gaseous mercury (GEM), gaseous oxidized mercury (GOM), and particulate bounded mercury (PBM). Knowledge on the anthropogenic and natural emissions of Hg to the atmosphere is important to better understanding of Hg fate in the natural environment (Lindberg et al., 2007). Since the late 1980s, studies have been carried out to investigate the spatial and temporal characteristics of Hg emissions from anthropogenic (Nriagu, 1989;Pirrone et al., 1996;Pacyna et al., 2003;Streets et al., 2005;Pacyna et al., 2010;Pirrone et al., 2010;Streets et al., 2009) and natural sources (Lindberg et al., 1998;Gustin et al., 1999;Gustin et al., 2000;Gustin, 2003;Shetty et al., 2008). Improved emission factors for estimating Hg release from different source categories have significantly reduced the uncertainties (typically <40%) of recently reported anthropogenic emissions (Lindberg et al., 2007;Pacyna et al., 2010;Pirrone et al., 2010). The natural emissions (including primary natural emissions and re-emissions of historically deposited Hg), however, still have large uncertainties due to poor understanding of process mechanisms and a lack of reliable data on Hg^0 air-surface exchange (Gustin et al., 2005;Schroeder et al., 2005;Selin et al., 2007;Zhang et al., 2009).

Asia is the largest anthropogenic source region of Hg. It contributes approximately two-thirds of global total anthropogenic Hg emissions (Pacyna et al., 2010;Pirrone et al., 2010). Significant progresses have been made in the estimate of anthropogenic Hg emissions in China (Streets et al., 2005;Wu et al., 2006;Tian et al., 2011;Liang et al., 2013). The most recent estimate suggests that total anthropogenic Hg emissions in China increased to 1028 tons in 2007 (Liang et al., 2013), nearly twofold higher than that in 1995 (Streets et al., 2005). In contrast, anthropogenic Hg emissions in other Asian countries (e.g. South Asia, Southeast Asia, and Central Asia) have received little attention. Such a lack of information limits the development of Hg emission inventories in a globally important source region. Due to the rapid economic development, anthropogenic Hg emissions in these regions are expected to considerably contribute to the regional Hg release (Pacyna et al., 2010).

Estimation of Hg emissions using observed concentrations of atmospheric GEM and other trace gases is a relatively novel approach for studying regional atmospheric Hg budgets. This method was firstly employed for estimating GEM emissions in the northeast USA using the GEM/CO_2 correlation slopes (Lee et al., 2001). The approach was further improved and then applied for estimating Hg emissions in Asia, Europe, and South Africa (Jaffe et al., 2005;Slemr et

al., 2006;Brunke et al., 2012). Such a measurement-based method complements the regional emission inventories estimated by conventional statistical approaches. It also yields an estimate of total Hg emissions from both anthropogenic and natural sources (Jaffe et al., 2005;Slemr et al., 2006). In the present study, the correlations slopes of GEM/CO, GEM/CO_2, and GEM/CH_4 were investigated using the long-term atmospheric measurements at three remote stations in northwest and southwest China. The correlation slopes were classified into four source regions in Asia (mainland China, South Asia, Indochinese Peninsula, and Central Asia) through trajectory analysis for estimating atmospheric Hg emissions. This work is aimed to fill the knowledge gaps in our understanding on Asian Hg emissions.

2 Experimental

2.1 Observational sites

In this study, observations were conducted at three remote sites in northwest and southwest China: Mt. Waliguan Baseline Observatory, Shangri-La station and Mt. Ailao station (Figure 1). The Mt. WLG Observatory (WLG, 100.898º E, 36.287º N, 3816 m a.s.l.) is one of the World Meteorological Organization's (WMO) Global Atmospheric Watch (GAW) Baseline Stations which is situated at the summit of Mt. Waliguan at the edge of northeast part of the Qinghai-Xizang (Tibet) Plateau. WLG is relatively isolated from industrial point sources and populated regions. The surrounding areas of WLG are naturally preserved arid/semi-arid lands and scattered grasslands and there is no local Hg source around the station. Most of the Chinese industrial and populated regions which may be related to anthropogenic Hg emissions are situated to the east of WLG. Due to the influence of Qinghai-Tibet Plateau monsoon, the predominate wind directions are from west to southwest sector in cold seasons and east sector in warm seasons, respectively. As shown in Figure 1, the three provinces including Qinghai, Xinjiang and Xizang have fairly low anthropogenic emissions of Hg, CO, CO_2, and CH_4 relative to eastern China, Central Asia and South Asia (Wu et al., 2006;Zhao et al., 2012b;Zhao et al., 2012a;Zhang et al., 2014a;Kurokawa et al., 2013). Therefore, anthropogenic emissions in these three Chinese provinces are expected to have minimal effect on the westerly and southwesterly airflows in cold seasons, which in turn largely reflect the feature of long-range atmospheric transport of air pollutants from Central Asia and South Asia to the WLG.

The Shangri-La station (XGL, 99.733º E, 28.017º N, 3580 m a.s.l.) is located in Hengduan Mountain area in the southeast Tibetan Plateau, southwest China (Figure 1). The minimal distance from the XGL station to South Asia and Indochinese Peninsula are 260 km and 100 km, respectively. The XGL station is surrounded by naturally preserved forest and mountainous areas. There are no large point sources within 100 km of the station with the exception of Shangri-La city,

which situates 30 km to the south of the station with a population of about 140,000 and may be related to anthropogenic emissions of Hg and other air pollutants. Areas to the west and south of the station are well preserved mountainous forest and have no significant anthropogenic sources. The long-range transport of air masses from South Asia and Indochinese Peninsula to the XGL station is not likely impacted by these areas.

The Mt. Ailao station (MAL, 100.017º E, 24.533º N, 2450 m a.s.l.) is located at a summit of the north side of Ailao Mountain National Nature Reserve in central Yunnan province, southwest China. The MAL Reserve stretches more than 130 km from south to north with a maximum width of approximately 20 km. More than 85% of the MAL Reserve is covered by preserved forest. MAL is isolated from industrial sources and populated regions in China. Kunming, one of the largest cities in southwest China, is located 180 km to the northeast of the station. The site is approximately 200 km and 600 km away from Indochinese Peninsula and South Asia approximately, respectively. Most of the Chinese anthropogenic sources of Hg and other air pollutants are located to the north and east to the station, whereas anthropogenic emissions in southern and western Yunnan province are fairly low (Wu et al., 2006;Zhao et al., 2012b;Zhao et al., 2012a;Zhang et al., 2014a;Kurokawa et al., 2013). The wind system at the station is dominated by the India Summer Monsoon (ISM) in warm seasons and the westerlies surrounding the Tibetan Plateau in cold seasons. The ISM can carry air pollutants from Indochinese Peninsula and southern China while the westerlies carry air pollutants from South Asia.

2.2 Measurements of GEM, CO, CO_2, and CH_4

Continuous measurements of atmospheric GEM at the WLG, XGL, and MAL stations were conducted using an automated Hg vapour analyzer (Tekran 2537A/B). This analyzer has been used extensively for atmospheric TGM measurements worldwide (Ebinghaus et al., 1999;Munthe et al., 2001;Fu et al., 2012a). It combines the pre-concentration of TGM onto gold traps, thermal desorption and cold vapour atomic fluorescence spectrometry detection of GEM. The analyzer has two gold cartridges working in parallel. While one cartridge is collecting TGM, the other one is performing analysis of the collected TGM. The function of the cartridges is then reversed, allowing continuous sampling of ambient air. The analyzer was set up in a temperature-controlled laboratory (15-25 ºC). Ambient air was introduced to the inlet of the analyzer by using a 25 ft heated Teflon tube (50 ºC). Air particulate matters were removed by using two 45-mm diameter Teflon filters (pore size 0.2 μm), which were installed at the inlets of the sampling Teflon tube and analyzer, respectively. The analyzer was programmed to measure atmospheric TGM at the time resolution of 5 min at XGL and MAL and 10 min at WLG with a volumetric sampling flow rate of ~1.5 L min^{-1}. The data quality of the analyzer was controlled by periodic (every 25 hours)

automatic permeation source injections, and the internal permeation source was calibrated every 3-6 months (Fu et al., 2012a). Atmospheric TGM in general consists of GEM and GOM. In most cases of these study, GOM constitutes a small portion of TGM (<1%, (Fu et al., 2012a)) and a large fraction of GOM was expected to be captured by the sampling Teflon tube and soda lime trap installed at the inlet of Tekran 2537A/B analyzer (Fu et al., 2010a;Fu et al., 2012b). Hence, the atmospheric TGM measured herein was referred to as GEM throughout the paper. Concentrations of GEM are expressed in ng m^{-3} (STP) with standard temperature of 273.16 K and pressure of 1013 hPa.

Atmospheric CO_2 at WLG was measured using a Licor6251 non-dispersive infrared (NDIR) analyzer, CH_4 and CO were measured using a G1301 (Picarro, USA) and a G1302 (Picarro, USA) Cavity Ring Down Spectroscopy systems (CRDS), respectively. Atmospheric CO_2 and CH_4 at XGL were measured using the G1301 (Picarro, USA) CRDS and CO was measured by the G1302 (Picarro, USA) CRDS. Detailed information regarding the schematic of the analytical systems, air collections, calibrations, and data processing has been addressed in previous studies (Zhou et al., 2003;Fang et al., 2013). The analytical precisions for the atmospheric CO_2, CH_4, and CO measurements were approximately 0.07 μmol mol^{-1} (ppm), 1.5 nmol mol^{-1} (ppb), and 2.0 nmol mol^{-1} (ppb), respectively. Atmospheric CO concentrations at MAL were measured using a non-dispersive infrared instrument (Themo Environmental Instruments Model 48C) (Jaffe et al., 2005). Periodical zero air and standard CO gases measurements were conducted to ensure a precise measurements of atmospheric CO concentrations.

All data were averaged hourly for correlation analysis. At WLG, datasets were available from October 2007 to September 2009 for GEM and CO_2, from July 2008 to September 2009 for CH_4, and from January to September 2009 for CO. Datasets for GEM, CO_2, and CH_4 were available from July to October 2010 and from September to October 2010 for CO at XGL. Only GEM and CO were available at MAL from September 2011 to March 2013. Due to the exchange of CO_2 between atmosphere and forest canopy, atmospheric CO_2 concentrations at XGL exhibited strong diurnal variations. This had a significant impact on the correlation analysis between GEM and CO_2. In light of this, we did not study the correlation of GEM to CO_2 at XGL.

2.3 Method of correlation analysis

Correlation analysis between atmospheric compounds is a novel tool for studying regional emissions strength of atmospheric pollutants. It has been used for estimating emissions of many atmospheric pollutants with data in good agreement with established emissions inventories (Yokouchi et al., 2006;Worthy et al., 2009;Tohjima et al., 2014). This method was developed and firstly utilized for estimating Hg emissions in Asia using the correlation of GEM to CO during

Asian outflow events (Jaffe et al., 2005). Subsequently, correlation slopes between GEM and other trace gases such as CH_4, CO_2, and halocarbons were also developed (Slemr et al., 2006;Brunke et al., 2012). These methods base on the assumptions of no chemical and physical losses of air pollutants, constant emission ratios and constant background of air pollutants during atmospheric transport events (Jaffe et al., 2005). In this study, correlations between atmospheric GEM and CO, CO_2, and CH_4 were utilized to estimate GEM emissions from mainland China, South Asia, Indochinese Peninsula and Central Asia on the basis of continuous measurements of atmospheric GEM, CO, CO_2, and CH_4 WLG, XGL, and MAL. The three stations are located in remote areas of northwest and southwest China and have constant backgrounds of atmospheric pollutants (Fu et al., 2012a;Zhang et al., 2014b). Also, the transport time (typically less than 5 days) of air masses from the source regions to the stations is much shorter than the atmospheric lifetimes of GEM, CO, CO_2, and CH_4. The multiple correlation relationships help constrain the estimated GEM emissions.

Correlation analysis was conducted by computing the Pearson correlation (orthogonal least-square correlation) between GEM concentrations and CO, CO_2, and CH_4 concentrations independently during pollution events when air masses originated or passed over a source region consistently. These events had GEM concentrations enhanced by at least 0.5 ng m^{-3} and lasted for 8 - 24 hours. Correlation slopes were selected when linear positive correlation is significant ($p > 0.01$) with a correlation coefficient (r^2) > 0.5 (significant correlations with negative slopes were excluded). This criterion was to ensure the method assumptions are valid (Jaffe et al., 2005). Figure 2 shows the time series of atmospheric GEM, CO, CO_2, and CH_4 concentrations during the transport events from 30 January to 2 March in 2009. The temporal variations of GEM were not consistently correlated with those of the three air pollutants because these events were possible impacted by different sources that led to different relative emission strength of air pollutants. Therefore, the correlation slopes of GEM/CO, GEM/CO_2, and GEM/CH_4 were calculated individually in this study. In addition, CH_4/CO, CH_4/CO_2, and CO/CO_2 correlation slopes were calculated during pollution events with CH_4 and CO concentrations elevated by at least 10 ppb and 20 ppb, respectively on the basis of criterion mentioned for GEM/CO, GEM/CO_2, and GEM/CH_4 correlation slopes. These correlation slopes are useful for constraining CH_4, CO, and CO_2 emissions in the study regions.

2.4 Air mass trajectory calculation

To establish the relationships between the observed correlations slopes and the source regions in Asia, we calculated 5-day backward trajectories every 2 hours at each of the stations using the TrajStat Geographical Information System software and gridded meteorological data (Global Data

Assimilation System, GDAS1) from the U.S. National Oceanic and Atmospheric Administration (NOAA). The global gridded meteorological data has a horizontal resolution of 1 degree (360×180 grid cells) with 23 vertical levels from 1000 hPa to 20 hPa (Wang et al., 2009). These trajectories ended at a height of 500 m above ground at WLG, XGL, and MAL stations. The trajectory endpoints in each event were averaged to yield the transport pathway. The source area identified by the trajectory analysis was weighted by the correlation slope observed at the stations during the event.

It should be noted that occasionally the endpoints of the backward trajectories can pass over multiple regions. In this case, we attributed the correlation slopes to the most important source regions that the air masses travelled through. For example, most air masses originated from and passed over South Asia and Central Asia and ended at WLG also passed over the Chinese provinces of Xinjiang, Xizang, and Qinghai that have fairly low emissions of atmospheric GEM, CO, CO_2, and CH_4 (Wu et al., 2006;Kurokawa et al., 2013). It is therefore assumed that these air masses carried the emission signals from Central and South Asia. On the other hand, eastern and central China is an important source region of atmospheric GEM, CO, CO_2, and CH_4, and therefore the air masses passing over eastern and central China were assumed to carry the emission signals in China. For the XGL and MAL stations, the areas to the west and south of the stations in Yunnan province, southwest China have fairly low emissions of atmospheric GEM, CO, CO_2, and CH_4 (Wu et al., 2006;Kurokawa et al., 2013). The air masses passed over South Asia and Indochinese Peninsula were assumed to carry the emission signals from the two regions, respectively.

3 Results and discussion

3.1 Atmospheric GEM concentrations at WLG, XGL, and MAL and potential source regions

Averaged atmospheric GEM concentrations during the study period were 2.05±0.96 ng m^{-3} (Hourly means ranging from 0.40 to 14.58 ng m^{-3}, October 2007 to September 2009) for WLG, 2.52±0.70 ng m^{-3} (Hourly means ranging from 1.35 to 5.98 ng m^{-3}, from July to October 2010) for XGL, and 2.05±0.67 ng m^{-3} (Hourly means ranging from 0.89 to 6.26 ng m^{-3}, from September 2011 to March 2013) for MAL. The levels of atmospheric GEM at the three stations were relatively lower compared to those observed in North America and Europe (1.3-2.0 ng m^{-3}, (Sprovieri et al., 2010;Lan et al., 2012;Cole et al., 2013;Munthe et al., 2003)). Previous study by Fu et al. (2012a) at WLG suggested that long-range atmospheric transport of GEM from industrial and urbanized areas in northwest China and northwest India contributed significantly to the elevated GEM at WLG. For GEM at XGL, potential sources areas included North India, Myanmar, West Sichuan Province and West Yunnan Province (Zhang et al., 2014b). The potential source

areas varied with monsoon at MAL. During the ISM seasons (May to October), MAL was mainly impacted by emission of Hg from eastern Yunnan, western Guizhou, and southern Sichuan of China and the north part of Indochinese Peninsula. During non-ISM seasons, impact from India and Northwest part of Indochinese Peninsula increased and played an important role in elevated GEM observed at MAL (Zhang et al., manuscript under preparation).

3.2 Observed correlation slopes for the studied source regions

Using backward trajectory analysis, we assigned GEM/CO slopes into four regions, GEM/CO_2 into three regions, and GEM/CH_4 into four regions (Table 1). Histograms of GEM/CO, GEM/CO_2, and GEM/CH_4 slopes for the identified source regions were displayed in Figure 3. Most of the correlation slopes followed a log-normal distribution (Table 1). Hence, geometric means of the correlation slopes were used throughout the paper.

The geometric mean correlation slopes of GEM/CO for mainland China, South Asia, Indochinese Peninsula and Central Asia were 7.3±4.3 pg m^{-3}/ppb (1SD, n=37), 7.8±6.4 pg m^{-3}/ppb (1SD, n=40), 7.8±5.0 pg m^{-3}/ppb (1SD, n=34), and 13.4±9.5 pg m^{-3}/ppb (1SD, n=6), respectively. The observed correlation slopes in mainland China were associated to air masses originating from northwest, southwest, central, and southern China (Figure 4). The trajectories were simulated for a period of 5-day and therefore are expected to pass over most the mainland China because of the length of trajectories. As a result, these observed correlation slopes of GEM/CO for northwest, southwest, central, and southern China were likely representative of the emission from a majority of areal coverage of mainland China. The correlation slopes of GEM/CO observed for South Asia, Indochinese Peninsula, and Central Asia are also representative of these regions as the air masses passing over a majority of these regions (Figure 4).

GEM/CO correlation slopes were comparable among mainland China, South Asia, and Indochinese Peninsula (means range from 7.3 to 7.8 pg m^{-3}/ppb), but nearly twofold lower than the mean for Central Asia (mean=13.4±9.5 pg m^{-3}/ppb). This trend is consistent with the anthropogenic emission ratios of GEM to CO in different regions of Asia. Based on the published anthropogenic GEM and CO emissions inventories in Asia (Kurokawa et al., 2013;AMAP/UNEP, 2013;Wu et al., 2006), we calculated anthropogenic GEM/CO emission ratio to be 7.2 pg m^{-3}/ppb (5.8×10^{-6} g/g) for Central Asia, which is significantly higher than those for mainland China (2.7 pg m^{-3}/ppb (2.2×10^{-6} g/g)), South Asia (1.6 pg m^{-3}/ppb (1.3×10^{-6} g/g)), and Indochinese Peninsula (1.5 pg m^{-3}/ppb (1.2×10^{-6} g/g)) (Table 2). Although correlation slopes of GEM/CO were also likely influenced by secondary emissions of GEM (Jaffe et al., 2005;Slemr et al., 2006), the higher anthropogenic GEM/CO emission ratio in Central Asia partially explains the elevated correlation slopes of GEM/CO in the region. The GEM/CO correlation slopes for mainland China were

slightly higher than those (4.6-7.4 pg m^{-3}/ppb) for Chinese outflows observed at Hedo Station, Okinawa, Japan, Mt. Bachelor Observatory (MBO), West USA, Seoul, Korea and coastal flights observations (Jaffe et al., 2005;Weiss-Penzias et al., 2007;Choi et al., 2009;Pan et al., 2006;Friedli et al., 2004), but slightly lower than values (8.0 and 11.4 pg m^{-3}/ppb) observed in the air masses originated from and/or passed over eastern China (Friedli et al., 2004;Sheu et al., 2010) and those (8.2-12.8 pg m^{-3}/ppb) in the upper troposphere observed during the flights from Frankfurt, Germany to Guangzhou, southern China (Slemr et al., 2009;Slemr et al., 2014). The difference between the present study and literature values may reflect a regional emission difference. The correlation slopes calculated from the observations in mainland China were associated to air masses originated from and passed over northwest, southwest, central, and southern China (Figure 4), whereas those estimated in previous studies were associated with the air masses in eastern China. Furthermore, there may be impacts from recent changes in atmospheric sources of GEM, including the decreasing contributions of GEM emissions from domestic coal, agricultural residual and forest burning emissions to the total anthropogenic emissions in mainland China during the past decade (Wu et al., 2006;Liang et al., 2013). These sources were reported with relatively lower GEM/CO emission ratios compared to other industrial sources (Weiss-Penzias et al., 2007;Zhang et al., 2013). There are few studies regarding the correlation slopes of GEM/CO in South Asia, Indochinese Peninsula, and Central Asia except the GEM/CO correlation slope (5.0 pg m^{-3}/ppb) for the outflow from Indochinese Peninsula reported by Sheu et al. (2010).

The geometric means of GEM/CO_2 correlation slopes for mainland China, South Asia, and Central Asia were 248±119 (1SD, n=25), 270± 164(1SD, n=21), and 315±289 (1SD, n=13) pg m^{-3}/ppm, respectively. The GEM/CO_2 correlation slopes calculated from the observations in mainland China were associated with air masses originating from northwest and southwest China and from central China (Figure 5). The GEM/CO_2 correlation slopes associated with trajectories transported from South Asia predominantly came primarily from Pakistan and northwest India, covering a large area of Central Asia (Figure 5). The values of GEM/CO_2 correlation slopes also vary with regions, with the greatest geometric mean GEM/CO_2 for the Central Asia. The spatial pattern of GEM/CO_2 slopes appeared to be consistent with the anthropogenic emission ratios of GEM to CO_2 in Asia. Taking the anthropogenic emissions of GEM and CO_2 into account (Wu et al., 2006;Kurokawa et al., 2013;AMAP/UNEP, 2013), GEM/CO_2 emission ratios of anthropogenic sources were in the order of 5.1×10^{-8} ton/ton in Central Asia and 4.2×10^{-8} ton/ton in mainland China, and 3.9×10^{-8} ton/ton) in South Asia

The geometric means of the correlation slopes of GEM/CH_4 for mainland China, South Asia, Indochinese Peninsula and Central Asia were 33.3±30.4 (1SD, n=41), 27.4±31.0 (1SD, n=4), 23.5±15.3 (1SD, n=6), and 20.5±10.0 (1SD, n=6) pg m^{-3}/ppb, respectively. Forty-one GEM/CH_4

ratios were calculated in mainland China (26 at the WLG site and 15 at the XGL site). The correlation slopes of GEM/CH_4 at WLG were associated with the air masses from northwest China and those at XGL were associated to the air masses from Yunnan province, southwest China (Figure 6). The events of air transport from South Asia, Indochinese Peninsula, and Central Asia (4-6 slopes for each region) were relatively fewer. The air masses related to the slopes for South Asia and Indochinese Peninsula were from northwest India and Myanmar, respectively. The GEM/CH_4 ratios calculated from the observations in the air masses from different regions in mainland China varied significantly (Figure 6). The GEM/CH_4 ratios associated with the air masses from northwest China fell in the range of 14.6-208 pg m^{-3}/ppb (geometric mean=49 pg m^{-3}/ppb), significantly higher than those from southwest China (ranging from 8 to 69 pg m^{-3}/ppb, geometric mean=20 pg m^{-3}/ppb). The lower GEM/CH_4 values estimated from the air transport from southwest China is likely due to the CH_4 emissions from rice paddies and natural wetlands (Zhang and Chen, 2010;Chen et al., 2013;Zhang et al., 2014a). The anthropogenic release of GEM to the atmosphere in the region is of relatively smaller quantity (Fu et al., 2012c).

The geometric means of the correlation slopes of CH_4/CO for mainland China, South Asia, Indochinese Peninsula and Central Asia were 0.27±0.18 (1SD, n=81), 0.31±0.09 (1SD, n=9), 0.30±0.20 (1SD, n=13), and 0.20±0.11 (1SD, n=9) ppb/ppb, respectively. The geometric means of the correlation slopes of CH_4/CO_2 for mainland China, South Asia, and Central Asia were 6.8±4.0 (1SD, n=36), 7.3±2.7 (1SD, n=12), and 8.7±5.9 (1SD, n=9) ppb/ppm, respectively. The geometric means of the CO/CO_2 correlation slopes for mainland China, South Asia, and Central Asia were 29.0±20.8 (1SD, n=43), 22.5±20.7 (1SD, n=8), and 16.8±8.4 (1SD, n=8) ppb/ppm, respectively. The observed correlation slopes for CH_4/CO, CH_4/CO_2, and CO/CO_2 in the studied regions were higher than that obtained for South Africa (Brunke et al., 2012). Note that observed CH_4/CO and CH_4/CO_2 correlation slopes were lower than anthropogenic emission ratios of CH_4/CO and CH_4/CO_2, while observed CO/CO_2 correlation slopes were consistent with anthropogenic emission ratios of CO to CO_2 (with the exception of South Asia, Table 1 and Table 2). This indicates that the anthropogenic inventories may overestimate the CH_4 emissions in the studied regions.

3.3 Implications for atmospheric Hg emission sources in Asia

The correlation slopes of GEM/CO, GEM/CO_2, and GEM/CH_4 were similar in Asian regions. This indicates that the sources of atmospheric Hg were more or less similar among the four studied regions. The GEM/CO, GEM/CO_2, and GEM/CH_4 correlation slopes in Asian were higher than those observed in other regions. For example, the GEM/CO ratios in Europe, South Africa, and North America were in the range of 0.3-5.0 pg m^{-3}/ppb (Jaffe et al., 2005;Slemr et al., 2006;Brunke et al., 2012). For GEM/CO_2 ratios, previous studies reported a mean of 184 pg

m^{-3}/ppm for the northeast United States and 63 pg m^{-3}/ppm for South Africa (Lee et al., 2001;Brunke et al., 2012). The mean GEM/CH_4 ratios in Europe and South Africa were 3.9 and 3.6 pg m^{-3}/ppb, respectively (Slemr et al., 2006;Brunke et al., 2012), approximately one order of magnitude lower than those in Asia.

Non-ferrous metal smelting (zinc, lead, and gold production), coal combustion, cement production, mercury production are the 4 largest source categories of anthropogenic GEM emissions in mainland China. Emissions factors (EF) of CO and CO_2 from anthropogenic sources have been investigated extensively. In this study, the EFs of CO and CO_2 summarized from Zhao et al. (2012a) and Zhao et al. (2012b) were adopted for calculating GEM/CO and GEM/CO_2 emission ratios for anthropogenic sources. EFs of GEM from coal combustion, non-ferrous smelting, cement, primary mercury production, and large-scale gold production have also be reported (Streets et al., 2005;Wang et al., 2010;Li et al., 2010;Pacyna et al., 2010). The emission ratios of GEM/CH_4 were not estimated due to the fact that GEM and CH_4 do not have common emission sources. The estimated emission ratio of GEM/CO is 149 pg m^{-3}/ppb for zinc smelting, 120 pg m^{-3}/ppb for lead smelting, 0.6 pg m^{-3}/ppb for coal combustion, 0.3 pg m^{-3}/ppb for cement production, 6.7×10^3 pg m^{-3}/ppb for primary mercury production, and 870×10^3 pg m^{-3}/ppb for large-scale gold production. The estimated emission ratio of GEM/CO_2 is 48×10^3 pg m^{-3}/ppm for zinc smelting, 131×10^3 pg m^{-3}/ppm for lead smelting, 10 pg m^{-3}/ppm for coal combustion, and 36 pg m^{-3}/ppm for cement production, 190×10^3 pg m^{-3}/ppm for primary mercury production, and 240×10^5 pg m^{-3}/ppm for large-scale gold production. It should be pointed out that artisanal and small-scale gold and mercury productions are also important sources of atmospheric GEM in Asia (Pacyna et al., 2010;Muntean et al., 2014). These two sources are generally equipped with poor Hg-control devices and expected to produce much larger emission ratios of GEM/CO and GEM/CO_2 (Li et al., 2009;Muntean et al., 2014). Biomass burning (forest and grassland fires, crop residual burning, and crop residues and wood combustion) is also an important atmospheric GEM source in mainland China (Huang et al., 2011). The observed GEM/CO and GEM/CO_2 emission ratios for biomass burning were 0.6-2.1 pg m^{-3}/ppb and 109 pg m^{-3}/ppm, respectively (Brunke et al., 2001;Friedli et al., 2003;Weiss-Penzias et al., 2007;Ebinghaus et al., 2007). Given that non-ferrous smelting and mercury production are important sources of atmospheric GEM in Asia and have relatively higher GEM/CO and GEM/CO_2 emission ratios, the elevated GEM/CO and GEM/CO_2 correlation slopes in Asia are likely resulted from these emission sources. None of the GEM/CO and GEM/CO_2 emission ratios from anthropogenic sources agree consistently with the observed correlation slopes, indicating that the observed correlation slopes of GEM/CO and GEM/CO_2 were likely influenced by multiple sources including release from natural surfaces.

Anthropogenic emission alone is not able to fully explain the observed correlation slopes.

Based on the annual anthropogenic emission inventories of GEM, CO, CO_2, and CH_4, the emission ratios of GEM/CO, GEM/CO_2, and GEM/CH_4 were calculated and shown in Table 2. The anthropogenic emission ratios were all significantly lower than the correlation slopes of observed concentrations. The discrepancy was partially attributed to the facts that observed correlation slopes were not uniformly distributed within different regions and seasons which may be not adequate to represent the annual and overall characteristics of the emission ratios in the studied regions. Unfortunately, this reason cannot be evaluated further due to the lack of seasonal assessments on the GEM, CO, CO_2, and CH_4 emissions. In addition, it is speculated that contributions from soil emission of GEM may play a crucial role. Soil emission is an important source of atmospheric GEM (Pirrone et al., 2010). Due to the lack of soil GEM flux measurements in South Asia, Indochinese Peninsula, and Central Asia, the measurement in China was applied for the analysis. The measured soil GEM fluxes in southwest and southern China fell in the ranges of 19.2-132 ng m^{-2} h^{-1} (mean=49 ng m^{-2} h^{-1}) and 18.2-114 ng m^{-2} h^{-1} (mean=43 ng m^{-2} h^{-1}), respectively (Feng et al., 2005;Fu et al., 2008;Fu et al., 2012c). These values are significantly higher than those in Europe and North America (Zhang et al., 2001;Ericksen et al., 2006;Schroeder et al., 2005). Assuming the soil emissions of CO_2 in mainland China are comparable to those in Europe and North America, the elevated GEM emission fluxes from soil in China can lead to the GEM/CO and GEM/CO_2 correlation slopes in mainland China. Using the published CO_2 emission fluxes from subtropical arable soil (Lou et al., 2004), we calculated the soil GEM/CO_2 emission ratios to be 148-1070 pg m^{-3}/ppm (mean=370 pg m^{-3}/ppm). Given that soil does not release significant CO to the atmosphere (EC-JRC/PBL, 2011), soil emissions are expected to produce extremely high GEM/CO emission ratios. Rice paddies are sources of both GEM and CH_4. However, previous studies suggested that GEM emission fluxes from rice paddies were much lower compared to those of bare soils, in the range of 1.4-23.8 ng m^{-2} h^{-1} (Zhu et al., 2011;Fu et al., 2012c). The mean CH_4 emission flux in China has been recorded as high as 11.4 mg m^{-2} h^{-1} (Chen et al., 2013). This yields average GEM/CH_4 emission ratios of 0.1-1.5 pg m^{-3}/ppb from rice paddies. The low GEM/CH_4 emission ratios from rice paddies were opposite to our observations, indicating that it is not the cause for elevated GEM/CH_4 slopes in China. However, bare soils are not expected to release CH_4 and should produce extremely high GEM/CH_4 emission ratios. Given the larger areas and higher GEM fluxes of bare soils in China, elevated GEM/CH_4 correlation slopes in China are probably caused by dry soil GEM emissions.

3.4 Estimates of GEM emissions

GEM emissions in mainland China, South Asia, Indochinese Peninsula, and Central Asia were calculated using the GEM/CO, GEM/CO_2, and GEM/CH_4 correlation slopes obtained in the

present study and emissions of CO, CO_2, and CH_4 in Asian countries. Emissions of CO, CO_2, and CH_4 in South Asia, Indochinese Peninsula, and Central Asia were adopted from the study by Kurokawa et al. (2013), which in most cases are consistent with those reported by EDGAR 4.2 (EC-JRC/PBL, 2011). Emissions of CO, CO_2, and CH_4 in mainland China were adopted from Chinese studies (Table -3). The emissions of CO and CO_2 in these studies agree with others reported in the literature (EC-JRC/PBL, 2011;Kurokawa et al., 2013;Liu et al., 2013;Tohjima et al., 2014). The CH_4 emission (39.6×10^6 tons $year^{-1}$) used for mainland China in this study is significantly lower than those ($73.2\text{-}76.0\times10^6$ tons $year^{-1}$) reported by Kurokawa et al. (2013) and EDGAR 4.2 (EC-JRC/PBL, 2011) but similar to that (46.0×10^6 tons $year^{-1}$) predicted from CH_4/CO_2 correlations at Hateruma Island (Tohjima et al., 2014). The Chinese studies utilized optimized emission factors for many sources (e.g. coal mining, rice cultivation, enteric fermentation, etc.) and are expected to give a better prediction of CH_4 emissions in China (Cheng et al., 2011;Chen et al., 2013).

Annual GEM emissions estimated from GEM/CO correlation slopes were 1071, 470, 125, 54 tons yr^{-1} for mainland China, South Asia, Indochinese Peninsula, and Central Asia, respectively. The estimated GEM emissions from GEM/CO_2 correlation slopes are similar to those derived from GEM/CO correlation slopes, with annual GEM emissions of 1187, 340, and 90 tons yr^{-1} for mainland China, South Asia, and Central Asia (no correlation slopes were observed for Indochinese Peninsula). GEM emissions estimated from GEM/CH_4 correlation slopes were substantially higher than those derived from GEM/CO and GEM/CO_2 correlation slopes (Table 3). For example, the estimated GEM emission in China based on GEM/CH_4 ratios reached 1846 ton yr^{-1}, 55-72% higher than those estimated from GEM/CO and GEM/CO_2 ratios. Similarly, the estimated GEM emissions in South Asia, Indochinese Peninsula, and Central Asia from GEM/CH_4 ratios were 1.2-3.9 times greater than those estimated from GEM/CO and GEM/CO_2 ratios.

The discrepancy in GEM emissions might be caused by the following reasons. First, it was reported that CH_4 emissions in China and other Asian counties have larger uncertainties compared to CO and CO_2 emissions (Olivier et al., 2001 ;Kurokawa et al., 2013). Recent Chinese studies have suggested that the CH_4 emissions in China reported by previous studies were overestimated by a factor of ~2 (Zhang and Chen, 2010;Cheng et al., 2011;Chen et al., 2013;Kurokawa et al., 2013). This may also be the case for South Asia, Indochinese Peninsula, and Central Asia. As shown in Table 1 and Table 2, the observed CH_4/CO and CH_4/CO_2 correlation slopes for the studied regions were significantly higher than the emission ratios calculated on basis of published inventories, while CO/CO_2 correlation slopes were consistent with the emission ratios. This implies that previously reported CH_4 emissions in the studied regions were likely overestimated, which may partially explain the overestimated GEM emissions derived from GEM/CH_4

correlation slopes and CH_4 emissions. Secondly, we do not obtain substantial correlation slopes of GEM/CH_4, which might be not representative for the studied regions. Using mainland China for example, 26 out of 41 slopes were observed at WLG. The slopes were related to air masses originated from and/or passed over northwest China, which yielded a mean GEM/CH_4 correlation slope of 49±30.0 pg m^{-3}/ppb, significantly higher than that (20.0±19.1 pg m^{-3}/ppb) of the slopes from southwest China. The slopes associated with air masses from northwest China were expected to be predominantly influenced by emissions of GEM and CH_4 its proximity to the WLG. Previous studies have suggested that the anthropogenic emission ratios of GEM/CH_4 in northwest China were relatively higher than the values from other Chinese regions (Wu et al., 2006;Zhang et al., 2014a). Therefore, the large fraction of slopes obtained from northwest China was also responsible for overestimates of GEM emissions in the present study. Hence, it is speculated that GEM/CO, GEM/CO_2 correlation slopes may better depict the GEM emissions in Asia than GEM/CH_4 correlation slopes in the present study.

The estimated GEM emissions in mainland China, South Asia, Indochinese Peninsula, and Central Asia using GEM/CO and GEM/CO_2 ratios agree reasonably with the results of previous studies (Jaffe et al., 2005;Weiss-Penzias et al., 2007), but consistently greater than the reported anthropogenic GEM emissions (Table 3). The estimated GEM emissions in China are about 3-4 folds higher than the anthropogenic emission for 2003-2010 (Wu et al., 2006;AMAP/UNEP, 2013;Muntean et al., 2014), and those in South Asia, Indochinese Peninsula, and Central Asia are 2-5 folds higher than the anthropogenic emissions for 2010 (AMAP/UNEP, 2013). It is hypothesized that underestimate of anthropogenic GEM emissions, contributions of re-emission and natural emissions, uncertainties in fraction of Hg species in the inventory, conversion of Hg species during long-range transport are the causes of explain the discrepancy (Jaffe et al., 2005;Slemr et al., 2006). A recent study showed that the total anthropogenic Hg emissions in China have increased to 1028 tons in 2007, which is about 50% higher than that in 2003 and corresponds to a mean annual increasing rate of 10.6% (Wu et al., 2006;Liang et al., 2013). If this increasing rate is applied to the estimate of anthropogenic GEM emissions in 2003 (Wu et al., 2006), anthropogenic GEM emission in China is expected to be 800 tons for 2010. This value is significantly higher than the estimate in 2003 as well as the value (430 tons) from the UNEP report for 2010 (Wu et al., 2006;AMAP/UNEP, 2013). There are few studies on anthropogenic GEM emissions in South Asia, Indochinese Peninsula, and Central Asia. A previous study suggested that total Hg emission in India was about 253 tons in 2004 (Mukherjee et al., 2009). Assuming GEM accounting for 64% of total Hg emissions in India (Pacyna et al., 2003), the GEM emission in India for 2004 was estimated to be 162 tons, ~2 times greater compared to the estimate of 96 tons in South Asia (including India and other South Asia countries) for 2010 by the

UNEP report (AMAP/UNEP, 2013). Given the increasing energy consumption recently, an increase in GEM emissions in South Asia is expected. This indicates the UNEP report for 2010 may underestimated GEM emissions in South Asia significantly.

Emission and reemission of GEM from natural sources were regarded as an important cause for the discrepancy between estimated GEM emissions using atmospheric pollutants correlation slopes and anthropogenic emission inventories (Jaffe et al., 2005;Slemr et al., 2006). Figure 7 shows the statistical summary of GEM exchange fluxes between different landscapes and atmosphere in warm season (from May to Oct) in mainland China. The mean GEM flux from dry farmland, rice paddies, grassland, forest soil, waters, and urban soil in warm seasons were 33.6±34.6, 17.4±15.9, 11.4±11.1, 8.8±6.4, 6.1±4.4, and 35.3±43.1 ng m^{-2} h^{-1}, respectively. These are significantly higher compared to those observed from Europe and North America (Poissant and Casimir, 1998;Boudala et al., 2000;Schroeder et al., 2005;Ericksen et al., 2006;Kuiken et al., 2008;Choi and Holsen, 2009). GEM fluxes from different landscapes in cold seasons (from Nov to Apr) were relatively limited. Several studies found that GEM fluxes from dry farmland, forest soil, and lake waters were about 2.5-40 times (mean=6.5, n=18) lower than those in warm seasons (Wang et al., 2003;Ma et al., 2013;Fu et al., 2010b;Fu et al., 2013). Given the different landscapes and seasonal patterns of GEM fluxes in mainland China, we estimate the annual natural GEM emissions to be 528 tons in China. This value is close to the estimate made by Shetty et al. (2008) but highlights the GEM emissions from dry farmland and grassland. There is no information regarding GEM fluxes from landscape in South Asia, Indochinese Peninsula, and Central Asia. Here we assume that the natural GEM fluxes from landscapes in these areas are similar to those in China and the annual GEM emissions from South Asia, Indochinese Peninsula, and Central Asia could be roughly estimated to be 240, 113, and 220 tons, respectively.

Uncertainties and limitations related to the correlation slope method may also be important for the discrepancy between estimated GEM emissions and anthropogenic emission inventories. These uncertainties and limitations may include the uncertainties of CO, CO_2, and CH_4 emissions as well as the limitations of observed correlation slopes. The uncertainties for CO_2 and CO emissions in China in Table 3 were estimated to be about 11% and 45%, respectively (Zhao et al., 2012a;Zhao et al., 2012b). Uncertainties for Chinese CH_4 emissions were not calculated by Zhang and Chen (2010) but expected to have much larger values (Kurokawa et al., 2013). The uncertainties for CO_2, CO, and CH_4 emissions in South Asia, Indochinese Peninsula, and Central Asia in Table 3 were estimated to be 44-49%, 114-131%, and 154-204%, respectively (Kurokawa et al., 2013). The limitations related to the correlation slopes were mainly caused by the fact that some of the emissions sources and pollution control devices of GEM, CO_2, CO, and CH_4 are not different, and this is a particular issue for GEM/CH_4 correlation slopes. It possibly resulted in

temporal and spatial variations of emission ratios between GEM and CO_2, CO, and CH_4. As shown in section 3.2 and 3.3, GEM/CO and GEM/CH_4 correlation slopes for mainland China observed at Mt. Waliguan (mainly related to air masses from northern and northwest China) were 66% and 145%, respectively higher than that observed at Shangri-La and Mt. Ailao (mainly related to air masses from southern and southwest China), and this may reflect the spatial variations of correlation slopes in China. A seasonally dependent variation of GEM/CO correlation slopes in the upper troposphere of China was also observed (Slemr et al., 2009). It is speculated that the temporal and spatial variations of GEM/CO and GEM/CO_2 correlation slopes might be smaller than that of GEM/CH_4, mainly due to the fact that GEM, CO, and CO_2 have many common emission sources. Nevertheless, since the correlation slopes were not obtained uniformly within different seasons and regions of the studied regions, they may be important causes for the uncertainties and limitations of the correlation slope method. Therefore, more field observations are still needed in future to better constrain Hg emissions in Asia.

4 Conclusions

The correlation slopes of GEM/CO, GEM/CO_2, and GEM/CH_4 were calculated and applied for estimating the GEM emission from four important source regions in Asia using ground-based measurements at 3 remote sites in northwest and southwest China and backwards trajectory analysis. The values of GEM/CO, GEM/CO_2, and GEM/CH_4 correlation slopes varied with the source regions. The GEM/CO correlation slopes were comparable among mainland China, South Asia, and Indochinese Peninsula, with the geometric means in the range of 7.3-7.8 pg m^{-3}/ppb, but they are about twofold lower than that (mean=13.4±9.5 pg m^{-3}/ppb) in Central Asia. This is consistent with GEM/ CO_2 correlation slopes for Central Asia (mean=315 pg m^{-3}/ppm), South Asia (mean=270 pg m^{-3}/ppm), and mainland China (mean=248 pg m^{-3}/ppm). However, we observed a opposite spatial trend for GEM/CH_4 correlation slopes that showed the highest geometric mean of 33.3±30.4 pg m^{-3}/ppb in mainland China, followed by South Asia (mean=27.4±31.0 pg m^{-3}/ppb), Indochinese Peninsula (mean=23.5±15.3 pg m^{-3}/ppb), and Central Asia (mean=20.5±10.0 pg m^{-3}/ppb). Elevated GEM/CO and GEM/CO_2 correlation slopes in Central Asia were found to be consistent with anthropogenic emission ratios of GEM relative to CO and CO_2, indicating anthropogenic sources played an important role in the observed correlation slopes. The highest GEM/CH_4 correlation slopes in mainland China were likely due to the transport from northwest China where strong GEM emissions and weak CH_4 emissions occur in the region.

The observed GEM/CO, GEM/CO_2, and GEM/CH_4 correlation slopes in Asia regions were consistently higher than those reported for Europe, North America, and South Africa. This highlights GEM emissions from non-ferrous smelting, mercury mining, natural sources and

historical deposited mercury (re-emission) in Asia. Using the correlation slopes of GEM/CO, GEM/CO_2 and recent inventories of CO and CO_2 in Asia countries, GEM emissions in mainland China, South Asia, Indochinese Peninsula, and Centrals were estimated to be in the ranges of 1071-1181 tons, 340-470 tons, 125 tons, and 54-90 tons, respectively. These estimates were lower than those predicted by the GEM/CH_4 correlation slopes because of the large uncertainties of CH_4 emissions in Asia as well as insufficient observations of GEM/CH_4 correlation slopes. These factors may lead to the overestimate of GEM emissions. On the other hand, the estimates of GEM emissions in this study were much higher than those from recent anthropogenic GEM emission inventories. This discrepancy could be resulted from the underestimate of anthropogenic GEM emissions in Asia and GEM emissions from natural sources (including primary natural sources and re-emission of historical deposited mercury), and the uncertainties related to CO, CO_2, and CH_4 emissions and limitation of observed correlation slops. Our preliminary assessment showed an annual GEM emission of about 528 tons from natural sources in mainland China, and 113-240 tons for South Asia, Indochinese Peninsula, and Central Asia. Although large uncertainties exist, these estimates seem to explain the discrepancies between the calculated GEM emissions based on the observed correlation slopes and anthropogenic emissions of GEM.

Acknowledgement: This work was funded by the National "973" Program of China (2013CB430003); the National Science Foundation of China (41273145, 41473025, 41003051, 41175116); the Innovative Program (Special Foundation for Young Scientist) of The Chinese Academy of Sciences (KZCX2-EW-QN111), the European Commission through GMOS (project no, 265113), and the National "973" Program of China (2010CB950601). We also acknowledge J. Pacyna and an anonymous reviewer for their valuable suggestions on our original version of the article.

References:

AMAP/UNEP: Technical Background Report for the Global Mercury Assessment 2013, Arctic Monitoring and Assessment Programme, Oslo, Norway/UNEP Chemicals Branch, Geneva, Switzerland., vi + 263 pp., 2013.

Boudala, F. S., Folkins, I., Beauchamp, S., Tordon, R., Neima, J., and Johnson, B.: Mercury flux measurements over air and water in Kejimkujik National Park, Nova Scotia, Water Air Soil Poll, 122, 183-202, Doi 10.1023/A:1005299411107, 2000.

Brunke, E. G., Labuschagne, C., and Slemr, F.: Gaseous mercury emissions from a fire in the Cape Peninsula, South Africa, during January 2000, Geophys Res Lett, 28, 1483-1486, Doi 10.1029/2000gl012193, 2001.

Brunke, E. G., Ebinghaus, R., Kock, H. H., Labuschagne, C., and Slemr, F.: Emissions of mercury in southern Africa derived from long-term observations at Cape Point, South Africa, Atmos Chem Phys, 12, 7465-7474, DOI 10.5194/acp-12-7465-2012, 2012.

612 Chen, H., Zhu, Q. A., Peng, C. H., Wu, N., Wang, Y. F., Fang, X. Q., Jiang, H., Xiang, W. H., Chang, J.,
613 Deng, X. W., and Yu, G. R.: Methane emissions from rice paddies natural wetlands, lakes in China:
614 synthesis new estimate, Global Change Biol, 19, 19-32, Doi 10.1111/Gcb.12034, 2013.
615 Cheng, Y. P., Wang, L., and Zhang, X. L.: Environmental impact of coal mine methane emissions and
616 responding strategies in China, Int J Greenh Gas Con, 5, 157-166, DOI 10.1016/j.ijggc.2010.07.007,
617 2011.
618 Choi, E. M., Kim, S. H., Holsen, T. M., and Yi, S. M.: Total gaseous concentrations in mercury in Seoul,
619 Korea: Local sources compared to long-range transport from China and Japan, Environ Pollut, 157,
620 816-822, DOI 10.1016/j.envpol.2008.11.023, 2009.
621 Choi, H. D., and Holsen, T. M.: Gaseous mercury fluxes from the forest floor of the Adirondacks,
622 Environ Pollut, 157, 592-600, DOI 10.1016/j.envpol.2008.08.020, 2009.
623 Cole, A. S., Steffen, A., Pfaffhuber, K. A., Berg, T., Pilote, M., Poissant, L., Tordon, R., and Hung, H.:
624 Ten-year trends of atmospheric mercury in the high Arctic compared to Canadian sub-Arctic and
625 mid-latitude sites, Atmos Chem Phys, 13, 1535-1545, DOI 10.5194/acp-13-1535-2013, 2013.
626 Ebinghaus, R., Jennings, S. G., Schroeder, W. H., Berg, T., Donaghy, T., Guentzel, J., Kenny, C., Kock,
627 H. H., Kvietkus, K., Landing, W., Muhleck, T., Munthe, J., Prestbo, E. M., Schneeberger, D., Slemr, F.,
628 Sommar, J., Urba, A., Wallschlager, D., and Xiao, Z.: International field intercomparison measurements
629 of atmospheric mercury species at Mace Head, Ireland, Atmos Environ, 33, 3063-3073, Doi
630 10.1016/S1352-2310(98)00119-8, 1999.
631 Ebinghaus, R., Slemr, F., Brenninkmeijer, C. A. M., van Velthoven, P., Zahn, A., Hermann, M.,
632 O'Sullivan, D. A., and Oram, D. E.: Emissions of gaseous mercury from biomass burning in South
633 America in 2005 observed during CARIBIC flights, Geophys Res Lett, 34, Artn L08813
634 Doi 10.1029/2006gl028866, 2007.
635 EC-JRC/PBL: European Commission, Joint Research Center/Netherlands Environmental Assessment
636 Agency, Emission Database for Global Atmospheric Research (EDGAR), release version 4.2, available
637 at: http://edgar.jrc.ec.europa.eu/index.php (last access: 4 October 2012), 2011.
638 Ericksen, J. A., Gustin, M. S., Xin, M., Weisberg, P. J., and Fernandez, G. C. J.: Air-soil exchange of
639 mercury from background soils in the United States, Sci Total Environ, 366, 851-863, DOI
640 10.1016/j.scitotenv.2005.08.019, 2006.
641 Fang, F. M., Wang, Q. C., and Li, J. F.: Urban environmental mercury in Changchun, a metropolitan
642 city in Northeastern China: source, cycle, and fate, Sci Total Environ, 330, 159-170, DOI
643 10.1016/j.scitotenv.2004.04.006, 2004.
644 Fang, S. X., Zhou, L. X., Masarie, K. A., Xu, L., and Rella, C. W.: Study of atmospheric CH4 mole
645 fractions at three WMO/GAW stations in China, J Geophys Res-Atmos, 118, 4874-4886, Doi
646 10.1002/Jgrd.50284, 2013.
647 Feng, X. B., Yan, H. Y., Wang, S. F., Qiu, G. L., Tang, S. L., Shang, L. H., Dai, Q. J., and Hou, Y. M.:
648 Seasonal variation of gaseous mercury exchange rate between air and water surface over Baihua
649 reservoir, Guizhou, China, Atmos Environ, 38, 4721-4732, DOI 10.1016/j.atmosenv.2004.05.023,
650 2004.
651 Feng, X. B., Wang, S. F., Qiu, G. A., Hou, Y. M., and Tang, S. L.: Total gaseous mercury emissions
652 from soil in Guiyang, Guizhou, China, J Geophys Res-Atmos, 110, Artn D14306
653 Doi 10.1029/2004jd005643, 2005.
654 Friedli, H. R., Radke, L. F., Prescott, R., Hobbs, P. V., and Sinha, P.: Mercury emissions from the
655 August 2001 wildfires in Washington State and an agricultural waste fire in Oregon and atmospheric

mercury budget estimates, Global Biogeochem Cy, 17, Artn 1039
Doi 10.1029/2002gb001972, 2003.
Friedli, H. R., Radke, L. F., Prescott, R., Li, P., Woo, J. H., and Carmichael, G. R.: Mercury in the atmosphere around Japan, Korea, and China as observed during the 2001 ACE-Asia field campaign: Measurements, distributions, sources, and implications, J Geophys Res-Atmos, 109, Artn D19s25
Doi 10.1029/2003jd004244, 2004.
Fu, X. W., Feng, X. B., Wang, S. F., Qiu, G. L., and Li, P.: Mercury flux rate of to Type s of grasslands in Guiyang, Research of Environmental Sciences (in Chinese with abstract in English), 20, 33-37, 2007.
Fu, X. W., Feng, X. B., and Wang, S. F.: Exchange fluxes of Hg between surfaces and atmosphere in the eastern flank of Mount Gongga, Sichuan province, southwestern China, J Geophys Res-Atmos, 113, Artn D20306
Doi 10.1029/2008jd009814, 2008.
Fu, X. W., Feng, X., Dong, Z. Q., Yin, R. S., Wang, J. X., Yang, Z. R., and Zhang, H.: Atmospheric gaseous elemental mercury (GEM) concentrations and mercury depositions at a high-altitude mountain peak in south China, Atmos Chem Phys, 10, 2425-2437, 2010a.
Fu, X. W., Feng, X. B., Wan, Q., Meng, B., Yan, H. Y., and Guo, Y. N.: Probing Hg evasion from surface waters of two Chinese hyper/meso-eutrophic reservoirs, Sci Total Environ, 408, 5887-5896, DOI 10.1016/j.scitotenv.2010.08.001, 2010b.
Fu, X. W., Feng, X., Liang, P., Deliger, Zhang, H., Ji, J., and Liu, P.: Temporal trend and sources of speciated atmospheric mercury at Waliguan GAW station, Northwestern China, Atmos Chem Phys, 12, 1951-1964, DOI 10.5194/acp-12-1951-2012, 2012a.
Fu, X. W., Feng, X., Shang, L. H., Wang, S. F., and Zhang, H.: Two years of measurements of atmospheric total gaseous mercury (TGM) at a remote site in Mt. Changbai area, Northeastern China, Atmos Chem Phys, 12, 4215-4226, DOI 10.5194/acp-12-4215-2012, 2012b.
Fu, X. W., Feng, X. B., Zhang, H., Yu, B., and Chen, L. G.: Mercury emissions from natural surfaces highly impacted by human activities in Guangzhou province, South China, Atmos Environ, 54, 185-193, DOI 10.1016/j.atmosenv.2012.02.008, 2012c.
Fu, X. W., Feng, X. B., Guo, Y. N., Meng, B., Yin, R. S., and Yao, H.: Distribution and production of reactive mercury and dissolved gaseous mercury in surface waters and water/air mercury flux in reservoirs on Wujiang River, Southwest China, J Geophys Res-Atmos, 118, 3905-3917, Doi 10.1002/Jgrd.50384, 2013.
Gustin, M. S., Lindberg, S., Marsik, F., Casimir, A., Ebinghaus, R., Edwards, G., Hubble-Fitzgerald, C., Kemp, R., Kock, H., Leonard, T., London, J., Majewski, M., Montecinos, C., Owens, J., Pilote, M., Poissant, L., Rasmussen, P., Schaedlich, F., Schneeberger, D., Schroeder, W., Sommar, J., Turner, R., Vette, A., Wallschlaeger, D., Xiao, Z., and Zhang, H.: Nevada STORMS project: Measurement of mercury emissions from naturally enriched surfaces, J Geophys Res-Atmos, 104, 21831-21844, Doi 10.1029/1999jd900351, 1999.
Gustin, M. S., Lindberg, S. E., Austin, K., Coolbaugh, M., Vette, A., and Zhang, H.: Assessing the contribution of natural sources to regional atmospheric mercury budgets, Sci Total Environ, 259, 61-71, Doi 10.1016/S0048-9697(00)00556-8, 2000.
Gustin, M. S.: Are mercury emissions from geologic sources significant? A status report, Sci Total Environ, 304, 153-167, Pii S0048-9697(02)00565-X
Doi 10.1016/S0048-9697(02)00565-X, 2003.

Gustin, M. S., Engle, M., Ericksen, J., Xin, M., Krabbenhoft, D., Lindberg, S., Olund, S., and Rytuba, J.: New insights into mercury exchange between air and substrate, Geochim Cosmochim Ac, 69, A700-A700, 2005.

Huang, X., Li, M. M., Friedli, H. R., Song, Y., Chang, D., and Zhu, L.: Mercury Emissions from Biomass Burning in China, Environmental Science & Technology, 45, 9442-9448, Doi 10.1021/Es202224e, 2011.

Jaffe, D., Prestbo, E., Swartzendruber, P., Weiss-Penzias, P., Kato, S., Takami, A., Hatakeyama, S., and Kajii, Y.: Export of atmospheric mercury from Asia, Atmos Environ, 39, 3029-3038, DOI 10.1016/j.atmosenv.2005.01.030, 2005.

Kuiken, T., Zhang, H., Gustin, M., and Lindberg, S.: Mercury emission from terrestrial background surfaces in the eastern USA. Part I: Air/surface exchange of mercury within a southeastern deciduous forest (Tennessee) over one year, Appl Geochem, 23, 345-355, DOI 10.1016/j.apgeocliem.2007.12.006, 2008.

Kurokawa, J., Ohara, T., Morikawa, T., Hanayama, S., Janssens-Maenhout, G., Fukui, T., Kawashima, K., and Akimoto, H.: Emissions of air pollutants and greenhouse gases over Asian regions during 2000-2008: Regional Emission inventory in ASia (REAS) version 2, Atmos Chem Phys, 13, 11019-11058, DOI 10.5194/acp-13-11019-2013, 2013.

Lan, X., Talbot, R., Castro, M., Perry, K., and Luke, W.: Seasonal and diurnal variations of atmospheric mercury across the US determined from AMNet monitoring data, Atmos Chem Phys, 12, 10569-10582, DOI 10.5194/acp-12-10569-2012, 2012.

Lee, X., Bullock, O. R., and Andres, R. J.: Anthropogenic emission of mercury to the atmosphere in the northeast United States, Geophys Res Lett, 28, 1231-1234, Doi 10.1029/2000gl012274, 2001.

Li, G. H., Feng, X. B., Li, Z. G., Qiu, G. L., Shang, L. H., Liang, P., Wang, D. Y., and Yang, Y. K.: Mercury emission to atmosphere from primary Zn production in China, Sci Total Environ, 408, 4607-4612, DOI 10.1016/j.scitotenv.2010.06.059, 2010.

Li, P., Feng, X. B., Qiu, G. L., Shang, L. H., Wang, S. F., and Meng, B.: Atmospheric mercury emission from artisanal mercury mining in Guizhou Province, Southwestern China, Atmos Environ, 43, 2247-2251, DOI 10.1016/j.atmosenv.2009.01.050, 2009.

Liang, S., Xu, M., Liu, Z., Suh, S., and Zhang, T. Z.: Socioeconomic Drivers of Mercury Emissions in China from 1992 to 2007, Environmental Science & Technology, 47, 3234-3240, Doi 10.1021/Es303728d, 2013.

Lindberg, S., Bullock, R., Ebinghaus, R., Engstrom, D., Feng, X. B., Fitzgerald, W., Pirrone, N., Prestbo, E., and Seigneur, C.: A synthesis of progress and uncertainties in attributing the sources of mercury in deposition, Ambio, 36, 19-32, 2007.

Lindberg, S. E., Hanson, P. J., Meyers, T. P., and Kim, K. H.: Air/surface exchange of mercury vapor over forests - The need for a reassessment of continental biogenic emissions, Atmos Environ, 32, 895-908, Doi 10.1016/S1352-2310(97)00173-8, 1998.

Liu, F., Cheng, H. X., Yang, K., Zhao, C. D., Liu, Y. H., Peng, M., and Li, K.: Characteristics and influencing factors of mercury exchange flux between soil and air in Guangzhou City, J Geochem Explor, 139, 115-121, DOI 10.1016/j.gexplo.2013.09.005, 2014.

Liu, M., Wang, H., Wang, H., Oda, T., Zhao, Y., Yang, X., Zang, R., Zang, B., Bi, J., and Chen, J.: Refined estimate of China's CO2 emissions in spatiotemporal distributions, Atmos Chem Phys, 13, 10873-10882, DOI 10.5194/acp-13-10873-2013, 2013.

Lou, Y. S., Li, Z. P., Zhang, T. L., and Liang, Y. C.: CO2 emissions from subtropical arable soils of

744 China, Soil Biol Biochem, 36, 1835-1842, DOI 10.1016/j.soilbio.2004.05.006, 2004.
745 Ma, M., Wang, D. Y., Sun, R. G., Shen, Y. Y., and Huang, L. X.: Gaseous mercury emissions from
746 subtropical forested and open field soils in a national nature reserve, southwest China, Atmos Environ,
747 64, 116-123, DOI 10.1016/j.atmosenv.2012.09.038, 2013.
748 Mason, R. P., Fitzgerald, W. F., and Morel, F. M. M.: The Biogeochemical Cycling of Elemental
749 Mercury - Anthropogenic Influences, Geochim Cosmochim Ac, 58, 3191-3198, Doi
750 10.1016/0016-7037(94)90046-9, 1994.
751 Mukherjee, A. B., Bhattacharya, P., Sarkar, A., and Zevenhoven, R.: Mercury emissions from industrial
752 sources in India and its effects in the environment, Springer, New York, USA, 81-112, 2009.
753 Muntean, M., Janssens-Maenhout, G., Song, S. J., Selin, N. E., Olivier, J. G. J., Guizzardi, D., Maas, R.,
754 and Dentener, F.: Trend analysis from 1970 to 2008 and model evaluation of EDGARv4 global gridded
755 anthropogenic mercury emissions, Sci Total Environ, 494, 337-350, DOI
756 10.1016/j.scitotenv.2014.06.014, 2014.
757 Munthe, J., Wangberg, I., Pirrone, N., Iverfeldt, A., Ferrara, R., Ebinghaus, R., Feng, X., Gardfeldt, K.,
758 Keeler, G., Lanzillotta, E., Lindberg, S. E., Lu, J., Mamane, Y., Prestbo, E., Schmolke, S., Schroeder, W.
759 H., Sommar, J., Sprovieri, F., Stevens, R. K., Stratton, W., Tuncel, G., and Urba, A.: Intercomparison of
760 methods for sampling and analysis of atmospheric mercury species, Atmos Environ, 35, 3007-3017,
761 Doi 10.1016/S1352-2310(01)00104-2, 2001.
762 Munthe, J., Wangberg, I., Iverfeldt, A., Lindqvist, O., Stromberg, D., Sommar, J., Gardfeldt, K.,
763 Petersen, G., Ebinghaus, R., Prestbo, E., Larjava, K., and Siemens, V.: Distribution of atmospheric
764 mercury species in Northern Europe: final results from the MOE project, Atmos Environ, 37, S9-S20,
765 Doi 10.1016/S1352-2310(03)00235-8, 2003.
766 Nriagu, J. O.: A Global Assessment of Natural Sources of Atmospheric Trace-Metals, Nature, 338,
767 47-49, Doi 10.1038/338047a0, 1989.
768 Olivier, J. G. J., Berdowski, J. J. M., Peters, J. A. H., Bakker, J., Visschedijk, A. J. H., and Bloos, J. P. J.:
769 Applications of EDGAR including a description of EDGAR 3.2: reference database with trend data for
770 1970-1995, RIVM, Bilthoven. RIVM report 773301001/NRP report 410 200 051., 2001
771 Pacyna, E. G., Pacyna, J. M., Sundseth, K., Munthe, J., Kindbom, K., Wilson, S., Steenhuisen, F., and
772 Maxson, P.: Global emission of mercury to the atmosphere from anthropogenic sources in 2005 and
773 projections to 2020, Atmos Environ, 44, 2487-2499, DOI 10.1016/j.atmosenv.2009.06.009, 2010.
774 Pacyna, J. M., Pacyna, E. G., Steenhuisen, F., and Wilson, S.: Mapping 1995 global anthropogenic
775 emissions of mercury, Atmos Environ, 37, S109-S117, Doi 10.1016/S1352-2310(03)00239-5, 2003.
776 Pan, L., Woo, J. H., Carmichael, G. R., Tang, Y. H., Friedli, H. R., and Radke, L. F.: Regional
777 distribution and emissions of mercury in east Asia: A modeling analysis of Asian Pacific Regional
778 Aerosol Characterization Experiment (ACE-Asia) observations, J Geophys Res-Atmos, 111, Artn
779 D07109
780 Doi 10.1029/2005jd006381, 2006.
781 Pirrone, N., Keeler, G. J., and Nriagu, J. O.: Regional differences in worldwide emissions of mercury to
782 the atmosphere, Atmos Environ, 30, 2981-2987, Doi 10.1016/1352-2310(95)00498-X, 1996.
783 Pirrone, N., Cinnirella, S., Feng, X., Finkelman, R. B., Friedli, H. R., Leaner, J., Mason, R., Mukherjee,
784 A. B., Stracher, G. B., Streets, D. G., and Telmer, K.: Global mercury emissions to the atmosphere from
785 anthropogenic and natural sources, Atmos Chem Phys, 10, 5951-5964, DOI 10.5194/acp-10-5951-2010,
786 2010.
787 Poissant, L., and Casimir, A.: Water-air and soil-air exchange rate of total gaseous mercury measured at

788 background sites, Atmos Environ, 32, 883-893, Doi 10.1016/S1352-2310(97)00132-5, 1998.
789 Schroeder, W. H., Beauchamp, S., Edwards, G., Poissant, L., Rasmussen, P., Tordon, R., Dias, G.,
790 Kemp, J., Van Heyst, B., and Banic, C. M.: Gaseous mercury emissions from natural sources in
791 Canadian landscapes, J Geophys Res-Atmos, 110, Artn D18302
792 Doi 10.1029/2004jd005699, 2005.
793 Selin, N. E., Jacob, D. J., Park, R. J., Yantosca, R. M., Strode, S., Jaegle, L., and Jaffe, D.: Chemical
794 cycling and deposition of atmospheric mercury: Global constraints from observations, J Geophys
795 Res-Atmos, 112, Artn D02308
796 Doi 10.1029/2006jd007450, 2007.
797 Shetty, S. K., Lin, C. J., Streets, D. G., and Jang, C.: Model estimate of mercury emission from natural
798 sources in East Asia, Atmos Environ, 42, 8674-8685, DOI 10.1016/j.atmosenv.2008.08.026, 2008.
799 Sheu, G. R., Lin, N. H., Wang, J. L., Lee, C. T., Yang, C. F. O., and Wang, S. H.: Temporal distribution
800 and potential sources of atmospheric mercury measured at a high-elevation background station in
801 Taiwan, Atmos Environ, 44, 2393-2400, DOI 10.1016/j.atmosenv.2010.04.009, 2010.
802 Slemr, F., Ebinghaus, R., Simmonds, P. G., and Jennings, S. G.: European emissions of mercury
803 derived from long-term observations at Mace Head, on the western Irish coast, Atmos Environ, 40,
804 6966-6974, DOI 10.1016/j.atmosenv.2006.06.013, 2006.
805 Slemr, F., Ebinghaus, R., Brenninkmeijer, C. A. M., Hermann, M., Kock, H. H., Martinsson, B. G.,
806 Schuck, T., Sprung, D., van Velthoven, P., Zahn, A., and Ziereis, H.: Gaseous mercury distribution in
807 the upper troposphere and lower stratosphere observed onboard the CARIBIC passenger aircraft,
808 Atmos Chem Phys, 9, 1957-1969, 2009.
809 Slemr, F., Weigelt, A., Ebinghaus, R., Brenninkmeijer, C., Baker, A., Schuck, T., Rauthe-Schoch, A.,
810 Riede, H., Leedham, E., Hermann, M., van Velthoven, P., Oram, D., O'Sullivan, D., Dyroff, C., Zahn,
811 A., and Ziereis, H.: Mercury Plumes in the Global Upper Troposphere Observed during Flights with the
812 CARIBIC Observatory from May 2005 until June 2013, Atmosphere-Basel, 5, 342-369, Doi
813 10.3390/Atmos5020342, 2014.
814 Sprovieri, F., Pirrone, N., Ebinghaus, R., Kock, H., and Dommergue, A.: A review of worldwide
815 atmospheric mercury measurements, Atmos Chem Phys, 10, 8245-8265, DOI
816 10.5194/acp-10-8245-2010, 2010.
817 Streets, D. G., Hao, J. M., Wu, Y., Jiang, J. K., Chan, M., Tian, H. Z., and Feng, X. B.: Anthropogenic
818 mercury emissions in China, Atmos Environ, 39, 7789-7806, DOI 10.1016/j.atmosenv.2005.08.029,
819 2005.
820 Streets, D. G., Zhang, Q., and Wu, Y.: Projections of Global Mercury Emissions in 2050,
821 Environmental Science & Technology, 43, 2983-2988, Doi 10.1021/Es802474j, 2009.
822 Tian, H. Z., Zhao, D., He, M. C., Wang, Y., and Cheng, K.: Temporal and spatial distribution of
823 atmospheric antimony emission inventories from coal combustion in China, Environ Pollut, 159,
824 1613-1619, DOI 10.1016/j.envpol.2011.02.048, 2011.
825 Tohjima, Y., Kubo, M., Minejima, C., Mukai, H., Tanimoto, H., Ganshin, A., Maksyutov, S., Katsumata,
826 K., Machida, T., and Kita, K.: Temporal changes in the emissions of CH4 and CO from China
827 estimated from CH4/CO2 and CO/CO2 correlations observed at Hateruma Island, Atmos Chem Phys,
828 14, 1663-1677, DOI 10.5194/acp-14-1663-2014, 2014.
829 Wang, D. Y., He, L., Shi, X. J., Wei, S. Q., and Feng, X. B.: Release flux of mercury from different
830 environmental surfaces in Chongqing, China, Chemosphere, 64, 1845-1854, DOI
831 10.1016/j.chemosphere.2006.01.054, 2006.

Wang, S., Feng, X., and Qiu, G.: The study of mercury exchange rate between air and soil surface in Hongfeng reservoir region, Guizhou, PR China, J Phys Iv, 107, 1357-1360, Doi 10.1051/Jp4:20030553, 2003.

Wang, S. X., Zhang, L., Li, G. H., Wu, Y., Hao, J. M., Pirrone, N., Sprovieri, F., and Ancora, M. P.: Mercury emission and speciation of coal-fired power plants in China, Atmos Chem Phys, 10, 1183-1192, 2010.

Wang, Y. Q., Zhang, X. Y., and Draxler, R. R.: TrajStat: GIS-based software that uses various trajectory statistical analysis methods to identify potential sources from long-term air pollution measurement data, Environ Modell Softw, 24, 938-939, DOI 10.1016/j.envsoft.2009.01.004, 2009.

Weiss-Penzias, P., Jaffe, D., Swartzendruber, P., Hafner, W., Chand, D., and Prestbo, E.: Quantifying Asian and biomass burning sources of mercury using the Hg/CO ratio in pollution plumes observed at the Mount Bachelor Observatory, Atmos Environ, 41, 4366-4379, DOI 10.1016/j.atmosenv.2007.01.058, 2007.

Worthy, D. E. J., Chan, E., Ishizawa, M., Chan, D., Poss, C., Dlugokencky, E. J., Maksyutov, S., and Levin, I.: Decreasing anthropogenic methane emissions in Europe and Siberia inferred from continuous carbon dioxide and methane observations at Alert, Canada, J Geophys Res-Atmos, 114, Artn D10301 Doi 10.1029/2008jd011239, 2009.

Wu, Y., Wang, S. X., Streets, D. G., Hao, J. M., Chan, M., and Jiang, J. K.: Trends in anthropogenic mercury emissions in China from 1995 to 2003, Environmental Science & Technology, 40, 5312-5318, Doi 10.1021/Es060406x, 2006.

Yokouchi, Y., Taguchi, S., Saito, T., Tohjima, Y., Tanimoto, H., and Mukai, H.: High frequency measurements of HFCs at a remote site in east Asia and their implications for Chinese emissions, Geophys Res Lett, 33, Artn L21814
Doi 10.1029/2006gl026403, 2006.

Zhang, B., and Chen, G. Q.: Methane emissions by Chinese economy: Inventory and embodiment analysis, Energ Policy, 38, 4304-4316, DOI 10.1016/j.enpol.2010.03.059, 2010.

Zhang, B., Li, J. S., and Peng, B. H.: Multi-regional input-output analysis for China's regional CH4 emissions, Front Earth Sci-Prc, 8, 163-180, DOI 10.1007/s11707-014-0408-0, 2014a.

Zhang, H., Lindberg, S. E., Marsik, F. J., and Keeler, G. J.: Mercury air/surface exchange kinetics of background soils of the Tahquamenon River watershed in the Michigan Upper Peninsula, Water Air Soil Poll, 126, 151-169, Doi 10.1023/A:1005227802306, 2001.

Zhang, H., Fu, X. W., Lin, C. J., Wang, X., and Feng, X. B.: Observation and analysis of speciated atmospheric mercury in Shangri-la, Tibetan Plateau, China, Atmos. Chem. Phys. Discuss., 14, 11041-11074, 10.5194/acpd-14-11041-2014, 2014b.

Zhang, L., Wang, S. X., Wang, L., and Hao, J. M.: Atmospheric mercury concentration and chemical speciation at a rural site in Beijing, China: implications of mercury emission sources, Atmos Chem Phys, 13, 10505-10516, DOI 10.5194/acp-13-10505-2013, 2013.

Zhang, L. M., Wright, L. P., and Blanchard, P.: A review of current knowledge concerning dry deposition of atmospheric mercury, Atmos Environ, 43, 5853-5864, DOI 10.1016/j.atmosenv.2009.08.019, 2009.

Zhao, Y., Nielsen, C. P., and McElroy, M. B.: China's CO2 emissions estimated from the bottom up: Recent trends, spatial distributions, and quantification of uncertainties, Atmos Environ, 59, 214-223, DOI 10.1016/j.atmosenv.2012.05.027, 2012a.

Zhao, Y., Nielsen, C. P., McElroy, M. B., Zhang, L., and Zhang, J.: CO emissions in China:

876 Uncertainties and implications of improved energy efficiency and emission control, Atmos Environ, 49,
877 103-113, DOI 10.1016/j.atmosenv.2011.12.015, 2012b.
878 Zhou, L. X., Tang, J., Wen, Y. P., Li, J. L., Yan, P., and Zhang, X. C.: The impact of local winds and
879 long-range transport on the continuous carbon dioxide record at Mount Waliguan, China, Tellus B, 55,
880 145-158, DOI 10.1034/j.1600-0889.2003.00064.x, 2003.
881 Zhu, J. S., Wang, D. Y., Liu, X. A., and Zhang, Y. T.: Mercury fluxes from air/surface interfaces in
882 paddy field and dry land, Appl Geochem, 26, 249-255, DOI 10.1016/j.apgeochem.2010.11.025, 2011.
883 Zhu, J. S., Wang, D. Y., and Ma, M.: Mercury release flux and its influencing factors at the air-water
884 interface in paddy field in Chongqing, China, Chinese Sci Bull, 58, 266-274, DOI
885 10.1007/s11434-012-5412-8, 2013.
886
887

888 Table 1 Statistical summary of GEM/CO, GEM/CO_2, GEM/CH_4, CH_4/CO, CH_4/CO_2, and CO/CO_2
889 correlation slopes observed for mainland China, South Asia, Indochinese peninsula, and
890 Central Asia during the study period.

Correlation slopes	Identified regions	Slope						
		Range	Geomean	Mean	Median	1SD	N	Log-normal K-S test (p)
GEM/CO (pg m^{-3}/ppb) (8.0×10^{-4} g/g)	mainland China	1.4-19.6	7.3	8.4	7.5	4.3	37	0.96
	South Asia	1.5-31.6	7.8	9.6	7.8	6.4	40	0.92
	Indochinese Peninsula	2.8-28.0	7.8	8.9	8.4	5.0	34	0.94
	Central Asia	2.0-34.0	13.4	17.0	17.0	9.5	6	0.93
GEM/CO_2 (pg m^{-3}/ppm) (5.1×10^{-7} g/g)	mainland China	115-687	248	268	254	119	25	1.0
	South Asia	130-743	270	305	266	164	21	0.88
	Central Asia	167-1260	315	374	275	289	13	0.97
GEM/CH_4 (pg m^{-3}/ppb) (1.4×10^{-3} g/g)	mainland China	8.3-110	33.3	43.4	34.9	30.4	41	0.87
	South Asia	14.5-80.9	27.4	35.0	22.3	31.0	4	0.90
	Indochinese Peninsula	7.8-47.7	23.5	27.7	28.8	15.3	6	0.87
	Central Asia	10.9-39.0	20.5	22.2	18.7	10.0	6	0.85
CH_4/CO (ppb/ppb) (0.57 g/g)	mainland China	0.05-0.93	0.27	0.31	0.28	0.18	81	0.88
	South Asia	0.21-0.52	0.31	0.32	0.29	0.09	9	0.96
	Indochinese Peninsula	0.10-0.77	0.30	0.36	0.33	0.20	13	0.76
	Central Asia	0.13-0.45	0.20	0.24	0.22	0.11	9	0.95
CH_4/CO_2 (ppb/ppm) (0.36×10^{-3} g/g)	mainland China	2.96-24.5	6.8	7.5	6.4	4.0	36	0.86
	South Asia	5.05-12.3	7.3	7.6	6.8	2.7	12	0.28
	Central Asia	5.22-23.2	8.7	9.9	8.6	5.9	9	0.69
CO/CO_2 (ppb/ppm) (0.64×10^{-3} g/g)	mainland China	10.1-152	29.0	32.0	27.4	20.8	43	0.29
	South Asia	13.7-75.9	22.5	26.8	20.7	20.7	8	0.68
	Central Asia	5.7-30.9	16.8	16.4	14.5	8.4	8	0.89

891
892
893
894
895
896
897
898
899
900
901
902
903
904
905
906

Table 2 Anthropogenic emissions GEM, CO, CO_2, and CH_4 in mainland China, South Asia, Indochinese Peninsula, and Central Asia as well as estimated anthropogenic emission ratios.

Regions	Anthropogenic emissions				Estimated emission ratios					
	GEM (tons yr^{-1})	CO ($\times10^6$ tons yr^{-1})	CO_2 ($\times10^6$ tons yr^{-1})	CH_4 ($\times10^6$ tons yr^{-1})	GEM/CO (pg m^{-3}/ppb)	GEM/CO_2 (pg m^{-3}/ppm)	GEM/CH_4 (pg m^{-3}/ppb)	CH_4/CO (ppb/ppb)	CH_4/CO_2 (ppb/ppm)	CO/CO_2 (ppb/ppm)
Mainland China	394.9[a]	183.0[b]	9370[c]	39.6[d]	2.7	82.4	7.1	0.38	11.6	30.7
South Asia	96.3[a]	75.2[e]	2460[e]	39.3[e]	1.6	76.5	1.8	0.91	43.8	48.1
Indochinese Peninsula	24.4[a]	19.9[e]	557[e]	14.9[e]	1.5	85.7	1.2	1.31	73.5	56.2
Central Asia	28.8[a]	5.0[e]	562[e]	7.5[e]	7.2	102	2.8	2.62	36.7	14.0

[a](AMAP/UNEP, 2013)

b(Zhao et al., 2012b)

c(Zhao et al., 2012a)

d(Zhang and Chen, 2010)

e(Kurokawa et al., 2013)

Table 3 Estimates of GEM emissions from mainland China, South Asia, Indochinese peninsula, and Central Asia using the observed correlation slopes and CO, CO_2, and CH_4 inventories, and a comparison to anthropogenic inventories was also added.

Asian regions	CO emission ($\times 10^6$ tons year^{-1})	CO_2 emission ($\times 10^6$ tons year^{-1})	CH_4 emission ($\times 10^6$ tons year^{-1})	Estimated GEM emission (tons year^{-1})			Anthropogenic GEM emission (tons year^{-1})
				From GEM/CO slopes	From GEM/CO_2 slopes	From GEM/CH_4 slopes	
Mainland China	183[a]	9370[b]	39.6[c]	1071	1187	1846	375-430[e]
South Asia	75.2[d]	2461[d]	39.3[d]	470	340	575	96[f]
Indochinese Peninsula	20.0[d]	557[d]	15.0[d]	125	--	493	24[f]
Central Asia	5.0[d]	562[d]	7.5[d]	54	90	215	29[f]

[a](Zhao et al., 2012b)

[b](Zhao et al., 2012a)

[c](Zhang and Chen, 2010)

[d](Kurokawa et al., 2013)

[e](Wu et al., 2006;AMAP/UNEP, 2013;Muntean et al., 2014)

[f](AMAP/UNEP, 2013)

Figure 1 Locations of the three ground-based remote sites in northwest and southwest China as well as the annual anthropogenic GEM emission for studies Asian countries (Wu et al., 2006;AMAP/UNEP, 2013).

968 Figure 2 A typical example for the consistent variations of GEM, CO, CO_2, and CH_4 for the
969 period of from 30 January to 2 March 2009 at Mt. Waliguan station.

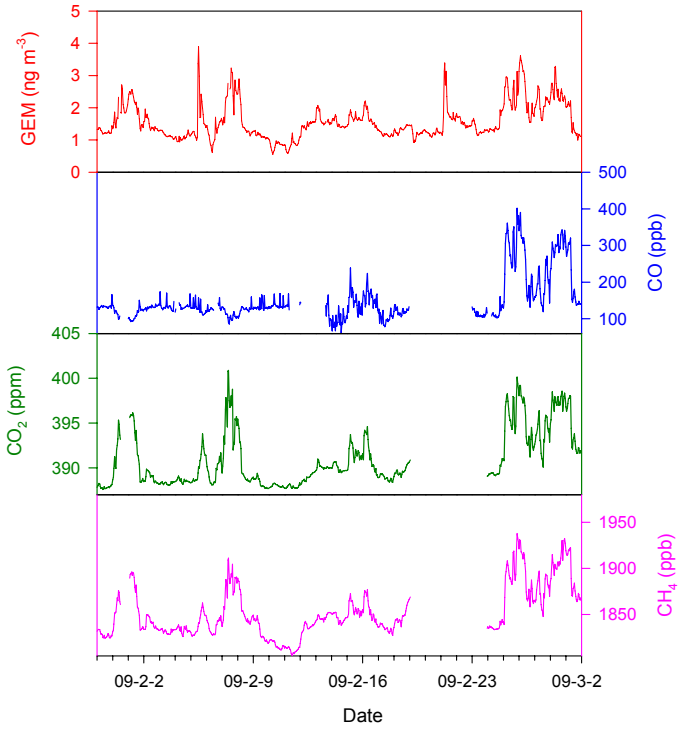

970
971
972
973

Figure 3 Histograms of the correlations slopes of GEM/CO, GEM/CO_2, and GEM/CH_4 for the four Asian regions during the whole study period. All the correlation slopes meet the selection criteria (see text).

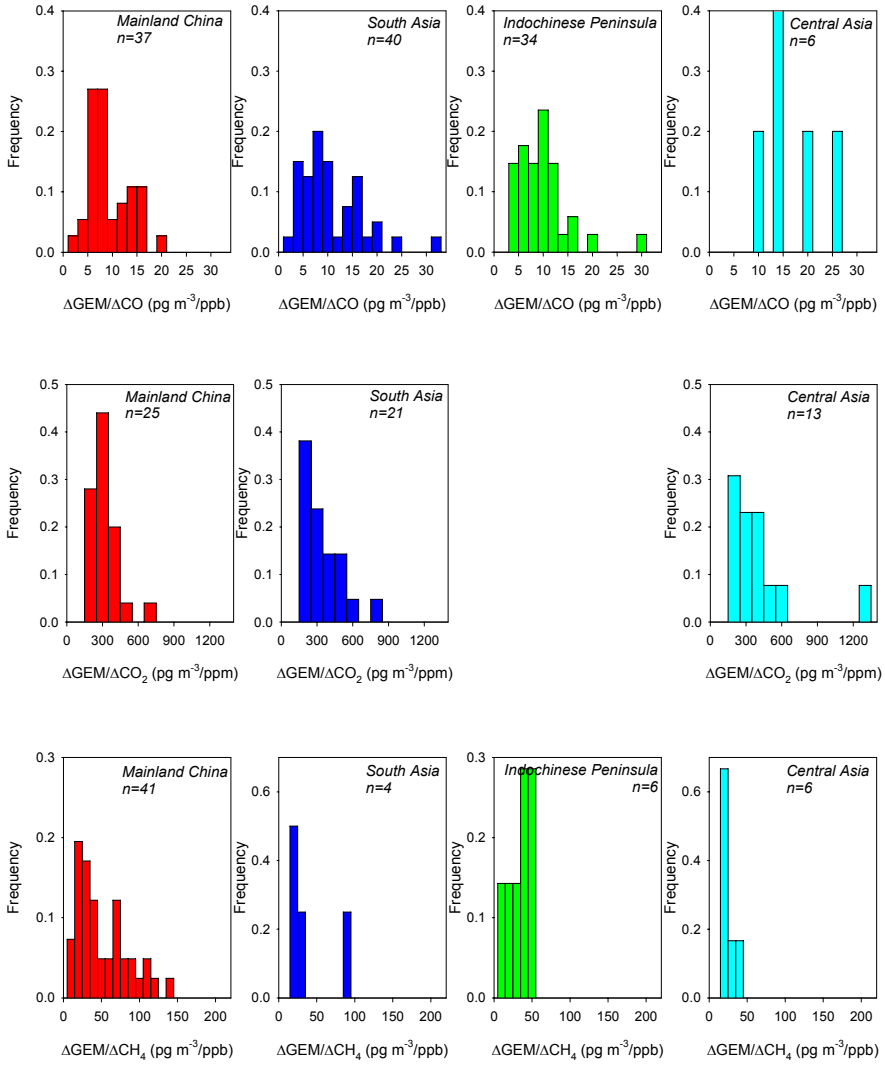

990 Figure 4 Correlation slopes of GEM/CO at the 3 monitoring sites and associated origins of
991 airflows.

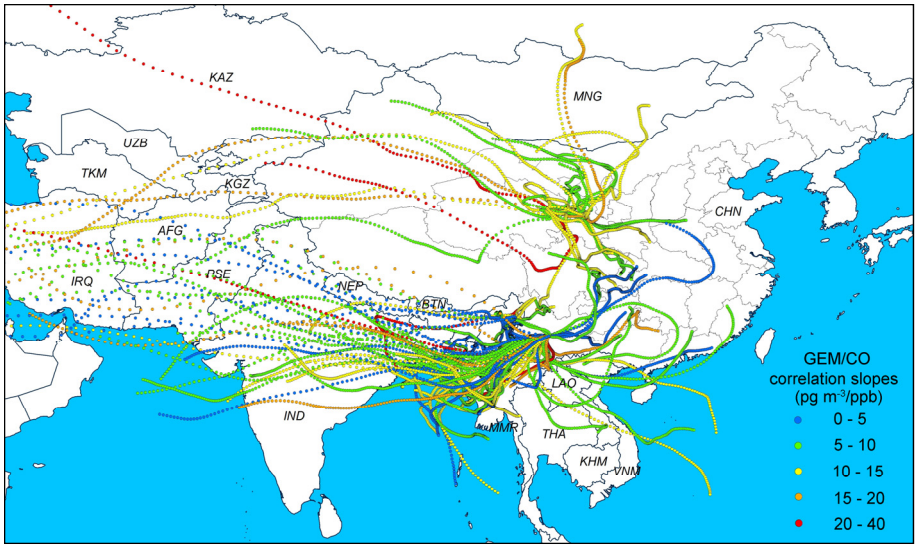

992

993

994

995 Figure 5 Correlation slopes of GEM/CO_2 at WLG and associated origins of airflows.

996

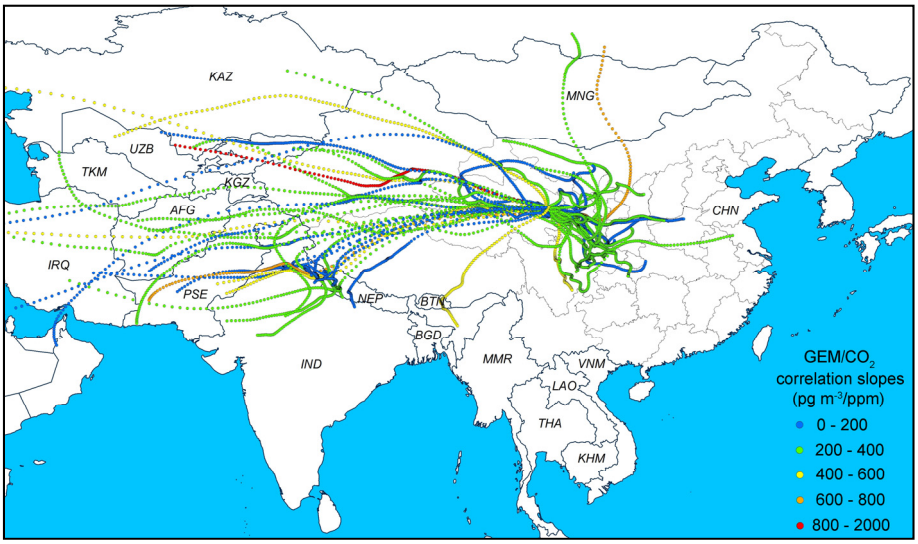

997

998

999 Figure 6 Correlation slopes of GEM/CH_4 at WLG and XGL and associated origins of
1000 airflows.

1001

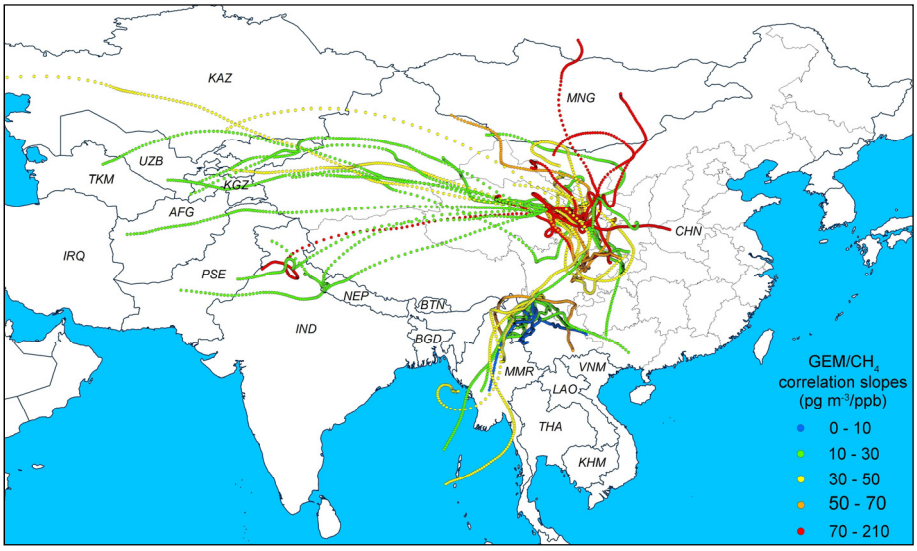

1002

1003

Figure 7 Statistical summary of GEM emission fluxes from typical landscapes in China in warm seasons (from May to Oct). The solid lines within each box represent the median fluxes, dashed line represents the mean, boundaries of the box represent 25th and 75th percentile, whiskers indicate 10th and 90th percentile, and plots indicate fluxes < 10th percentile or >90th percentile.

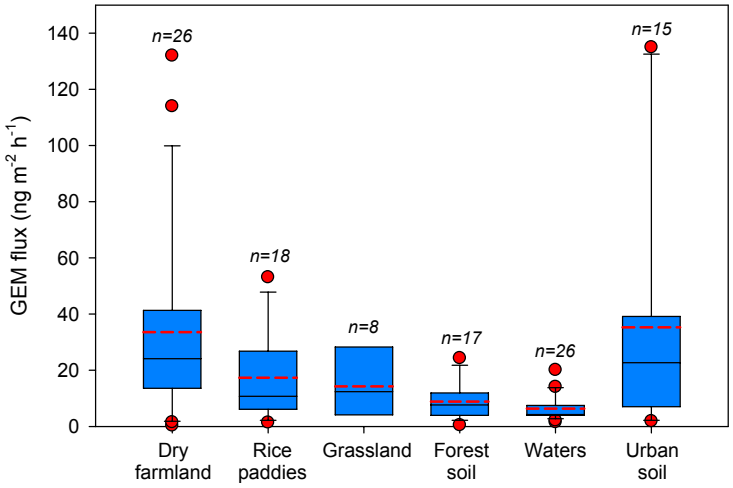

References: (Wang et al., 2003;Feng et al., 2004;Fang et al., 2004;Feng et al., 2005;Wang et al., 2006;Fu et al., 2008;Fu et al., 2007;Fu et al., 2010b;Zhu et al., 2011;Fu et al., 2012c;Fu et al., 2013;Ma et al., 2013;Zhu et al., 2013;Liu et al., 2014)